Polymer Solar Cells: Bithiophene Imide and Benzodithiophene Copolymers for Efficient Inverted Polymer Solar Cells (Adv. Mater. 17/2012)

ARTICLE *in* ADVANCED MATERIALS · MAY 2012

Impact Factor: 17.49 · DOI: 10.1002/adma.201103948 · Source: PubMed

8 AUTHORS, INCLUDING:

Xugang Guo
South University of Science and Technolog…
28 PUBLICATIONS **1,570** CITATIONS
SEE PROFILE

Rocio Ponce Ortiz
University of Malaga
69 PUBLICATIONS **2,438** CITATIONS
SEE PROFILE

Shiqiang Q Li
Northwestern University
10 PUBLICATIONS **124** CITATIONS
SEE PROFILE

Shiming Zhang
Huawei Technologies Co. Ltd.
20 PUBLICATIONS **774** CITATIONS
SEE PROFILE

ADVANCED MATERIALS
www.advmat.de

Materials Views
www.MaterialsViews.com

Bithiophene Imide and Benzodithiophene Copolymers for Efficient Inverted Polymer Solar Cells

Nanjia Zhou, Xugang Guo, Rocio Ponce Ortiz, Shiqiang Li, Shiming Zhang, Robert P. H. Chang, Antonio Facchetti,* and Tobin J. Marks**

Photovoltaic cells have received intensified research efforts in the past decades in both academia and industry, due to the increasing demand for sustainable clean energy. Among the types of cells, organic photovoltaic (OPV) cells offer promise due to the ease of materials processing and device mechanical flexibility. These characteristics should enable fabrication of light-weight, flexible devices using high-throughput printing techniques, thereby eliminating expensive vacuum technologies required for associated high temperature fabrication process.[1–3] Moreover, OPV performance has significantly advanced in the last few years through the design and synthesis of novel new active materials,[4,5] modified interfacial layers,[6,7] optimized film morphologies,[8,9] and engineered device architectures.[10,11] To date, power conversion efficiencies (PCEs) have risen to 7–8% in bulk heterojunction (BHJ) OPVs using polymer semiconductors as electron donors and fullerene derivatives as electron acceptors.[12–14] Nevertheless, while OPV PCEs have significantly increased in the past few years, their performance is still significantly below that of their inorganic counterparts,[15] and more intensive research will be required to further enhance the device performance.

Donor-acceptor (D-A) block strategies have been an important tool in designing new high-performance polymers for OPV applications since they allow effective tuning of both band gaps and frontier molecular orbital (FMO) energies.[16] Appropriate band gaps can maximize solar radiation capture to facilitate exciton formation, and suitable FMO energies can provide the driving force for efficient exciton dissociation at polymer donor/PCBM acceptor interfaces and also enhance open-circuit voltages (V_{oc}s).[17] Implementation of novel acceptor monomers to copolymerize with suitable electron donor co-units is attractive for optimizing processability, band gaps, and FMO energies.[18–20] As an electron acceptor unit, the thieno[3,4-*c*]pyrrole-4,6-dione fragment (TPD, structure shown in **Figure 1**) has attracted attention since the first report by Leclerc in 2010,[20,21] and TPD-based D-A polymers have achieved substantial OPV PCEs (4–7%) when combined with donor co-units such as benzodithiophene,[20,22] cyclopentadithiophene,[23] and dithienosilole.[24] Nevertheless, further development in organic photovoltaics will depend critically on the design and incorporation of new and useful building blocks into active layer polymer backbones, especially new electron-deficient units. This laboratory recently designed and synthesized a new bithiophene imide group (BTI, Figure 1) which demonstrates strong electron-withdrawing character, a planar architecture, and good solubility.[25] In that work, the BTI unit was used to construct homopolymers and D-A copolymers for organic thin-film transistors, and substantial electron and hole mobilities were achieved (>0.1 cm^2/Vs).[26] In comparison to TPD units, BTI units have the advantage of decreased steric encumberance achieved by placing the imide group at the center of BTI unit, and this should enable BTI copolymerization with a variety of comonomers to realize extended conjugation. The low HOMO energies and relatively small band gaps, combined with good solubilities, favorable geometries, and promising charge transport properties, raise the intriguing question of whether BTI-based polymers might be effective donor components of BHJ solar cells.

Benzodithiophene (BDT) is chosen here as the initial donor co-unit due to its solubilizing characteristics, effective tuning of the band gap, and appropriate FMO energies.[27] Moreover, density functional theory (DFT) calculations (Figure 1) indicate that the BTI-BDT copolymer repeat unit has a HOMO energy (–5.39 eV) similar to that of TPD-BDT copolymer repeat unit (–5.41 eV), presaging high solar cell V_{oc}s. We report here inverted bulk heterojunction (BHJ) BTI-based polymer solar cells with V_{oc}s higher than 0.9 V and PCEs up to 5.5%. The results indicate that BTI is a promising building block for constructing BHJ OPV polymer donors which will be explored further in future work.

The present BTI-BDT copolymers were synthesized as shown in **Scheme 1**. The dibrominated bithiophene imide monomer[26] and distannylated benzodithiophene comonomers[28] were prepared and purified as described in the Supporting Information. Differing alkyl substituents were employed to ensure solubility and to examine their effects on film morphology and device performance. Polymers **P1** and **P2** were synthesized via Stille coupling, and the resulting polymers endcapped with thiophene units,[29,30] followed by Soxhlet extraction to remove

N. Zhou, S. Li, Prof. R. P. H. Chang
Department of Materials Science and Engineering
the Argonne-Northwestern Solar Energy Research Center
the Materials Research Center
Northwestern University
2145 Sheridan Road, Evanston, Illinois, 60208, USA
E-mail: r-chang@northwestern.edu
Dr. X. Guo, Dr. R. P. Ortiz, Dr. S. Zhang,
Prof. A. Facchetti, Prof. T. J. Marks
Department of Chemistry
the Argonne-Northwestern Solar Energy Research Center
Northwestern University
2145 Sheridan Road, Evanston, Illinois, 60208, USA
E-mail: a-facchetti@northwestern.edu; t-marks@northwestern.edu

DOI: 10.1002/adma.201103948

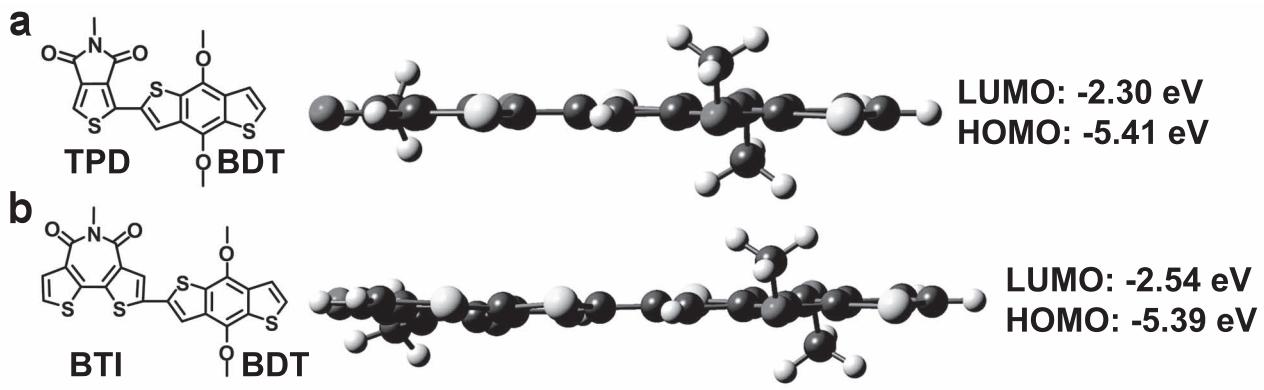

Figure 1. Chemical structures, planar geometries, and HOMO and LUMO energies of the TPD-BDT repeat units (a) and BTI-BDT repeat units (b) calculated at the DFT//B3LYP/6-31G** level. Alkyl chains are replaced by methyl groups to simplify the calculations.

low molecular weight fractions. Molecular weights measured by high temperature GPC show that **P1** has an M_n = 21.8 kDa (PDI = 3.28), while **P2** has an M_n = 34.0 kDa (PDI = 2.95). For polymer **P2**, in addition to straight chain *n*-dodecyl as the BDT substituent, the bulky BTI 2-hexyldecyl group is necessary for sufficient solubility at room temperature for device fabrication (>10 mg/mL). Using 2-butyloctyl as the BTI substituent results in poor solubility, however, the branched 2-ethylhexyl BDT substituent combined with the BTI 2-butyloctyl group affords adequate **P1** solubility. The present polymerizations produce **P1** and **P2** with acceptable molecular weights due to the good solubilities and efficient Pd-mediated coupling reactions. The structures and purities are supported by ^{1}H NMR spectra and elemental analysis (see the Supporting Information for details).

The optical properties of the BTI-based polymers were investigated by UV-visible absorption spectroscopy in solution and as-cast thin films; spectra are shown in **Figure 2**a. The absorption onsets of the as-cast **P1** and **P2** films are at 642 and 644 nm, respectively, with estimated optical band gaps of ~1.93 eV–about 0.1 eV larger than that of typical TPD-BDT copolymers.[20,28] The spectra of both **P1** and **P2** exhibit an absorption shoulder, similar to the vibronic profiles seen in the spectra of regioregular polythiophenes,[31] and indicative of polymer chain ordering in the solid film. For π-conjugated polymers it is known that intermolecular forces and conformational changes may considerably shift the optical absorption.[32] However, no significant differences are observed in the absorption profiles of both the present polymers on going from the solution to the film state. The absence of bathochromic shifts from solutions to films can be ascribed to the rigid polymer backbones enforced by the fused BTI and BDT subunits and probable pre-aggregation in solution. In OPVs, polymer FMO energies play a critical role in exciton dissociation and V_{oc},[17] and were measured here by cyclic voltammetry (CV; Figure 2b). The HOMO and LUMO energies, calculated from the onset of oxidation and reduction waves in cyclic voltammograms, are −5.58 eV and −3.50 eV for **P1**; and −5.63 eV and −3.43 eV for **P2**, respectively. The BTI unit electron-deficiency results in low-lying **P1** and **P2** HOMOs, consistent with the present DFT calculations (Figure 1). The band gaps derived from electrochemistry are slightly larger than the optical band gaps by 0.1 – 0.2 eV, doubtlessly reflecting the exciton binding energies of these organic semiconductors.[33] Thermal analysis of the **P1** and **P2** was carried out by thermogravimetric analysis (TGA) and differential scanning calorimetry (DSC) at a temperature ramp rate of 10 °C/min under N_2. The TGA data (Figure S1) indicate that **P1** and **P2** are robust with decomposition temperatures of 337 °C and 332 °C, respectively, defined as the temperature at 5% mass loss. No significant transition temperatures are detected in the DSC data up to 320 °C (Figure S2), in a good agreement with the amorphous characteristics as revealed by the film XRD data (Figure S3).

Inverted architectures were chosen to investigate the performance of BTI-based polymer solar cells, specifically ITO/ZnO/polymer:$PC_{71}BM$/MoO_x/Ag, as shown in **Figure 3**a. Inverted structures avoid oxidation of low work-function cathodes, such as Al or Ca, and acidic PEDOT:PSS etching of ITO, both of which limit conventional devices.[10,11] ZnO is an excellent cathode interfacial layer due to its high electron mobility, excellent thermal stability, and hole-blocking properties.[34,35] The 20 nm amorphous ZnO is processed at 150 °C via $Zn(OAc)_2$ hydrolysis, according to the protocol of Chou *et al.*[36] As a successful anode interfacial layer (IFL),[36,37] MoO_x is chosen here due to its environmental robustness, processability, and efficient hole-transport/electron-blocking properties.[36] An energy level diagram of the component materials used in the present inverted solar cells is

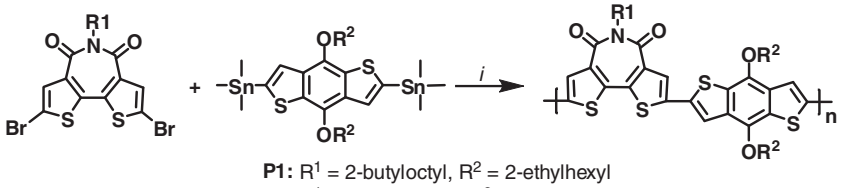

P1: R^1 = 2-butyloctyl, R^2 = 2-ethylhexyl
P2: R^1 = 2-hexyldecyl, R^2 = *n*-dodecyl

[a] Reagent and conditions: (*i*) $Pd_2(dba)_3$, P(*o*-tolyl)$_3$; Pd loading 0.03 equiv, toluene, 110 °C

Scheme 1. Synthetic Route to BTI-BDT Copolymers[a].

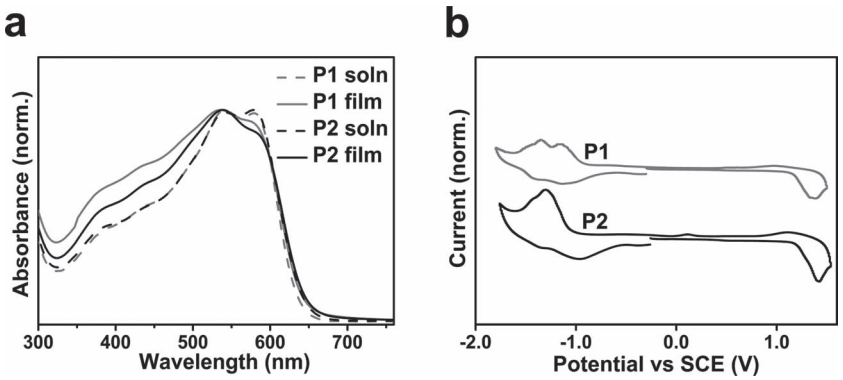

Figure 2. Optical absorption spectra (a) of bithiophene imide-based polymers **P1** (grey) and **P2** (black) in chlorobezene (dashed line, 1×10^{-5} M) and as pristine films (solid line) drop-cast from chlorobenzene solution (1 mg/mL). Cyclic voltammograms (b) of bithiophene imide-based polymer thin films measured in 0.1 M $(n\text{-Bu})_4N{\cdot}PF_6$ acetonitrile solution at scan rate of 50 mV/s.

shown in Figure 3b. The MoO_x conduction band (-2.60 eV) lies sufficiently above the donor LUMOs (–3.7 eV, estimated from the HOMOs and optical band gaps), to block electrons, while the low work function (–5.6 eV) forms a good anodic contact with the donor polymers for hole extraction.

The photovoltaic parameters of **P1**- and **P2**-based solar cells are summarized in **Table 1**. Cells were first investigated using *ortho*-dichlorobenzene (DCB) as the processing solvent. For optimized devices shown in Figure 3c, the **P1**:$PC_{71}BM$ = 1:1.5 and **P2**:$PC_{71}BM$ = 1:1 weight ratios afford optimum performance among the blend combinations. The **P1**-based solar cells exhibit V_{oc} = 0.992 V, J_{sc} = 4.16 mA/cm^2, and fill factor (*FF*) = 47.9%, with PCE = 1.98%. The **P2**-based solar cells show V_{oc} = 0.940 V, J_{sc} = 4.76 mA/cm^2, and *FF* = 56.3%, with PCE = 2.52%. The V_{oc} of BTI-based solar cells are among the highest V_{oc}s reported to date for polymer/PCBM solar cells,[5,21] in a good agreement with the low-lying HOMOs measured by cyclic voltammetry. Processing additives, such as 1,8-diiodooctane (DIO), have been used in BHJ OPVs to optimize the device performance by the promoting nano-scale phase separation.[9] Using DCB:DIO (97%:3%, v/v) as the processing solvent here significantly enhances performance in the **P1**-/**P2**-based OPVs. Thus, **P1**-based solar cells show V_{oc} = 0.876 V, J_{sc} = 9.69 mA/cm^2, and *FF* = 51.8% with a PCE = 4.39%. Furthermore, **P2**-based solar cells show V_{oc} = 0.922 V, J_{sc} = 9.62 mA/cm^2, and *FF* = 62.0% with a PCE = 5.50%. The PCEs of current inverted solar cells are lower than the best inverted solar cells reported by Reynolds[11] due to the lower J_{sc}s, which are mainly limited by the relatively large band gaps of these BTI-based polymers. Devices having other polymer/$PC_{71}BM$ blend ratios

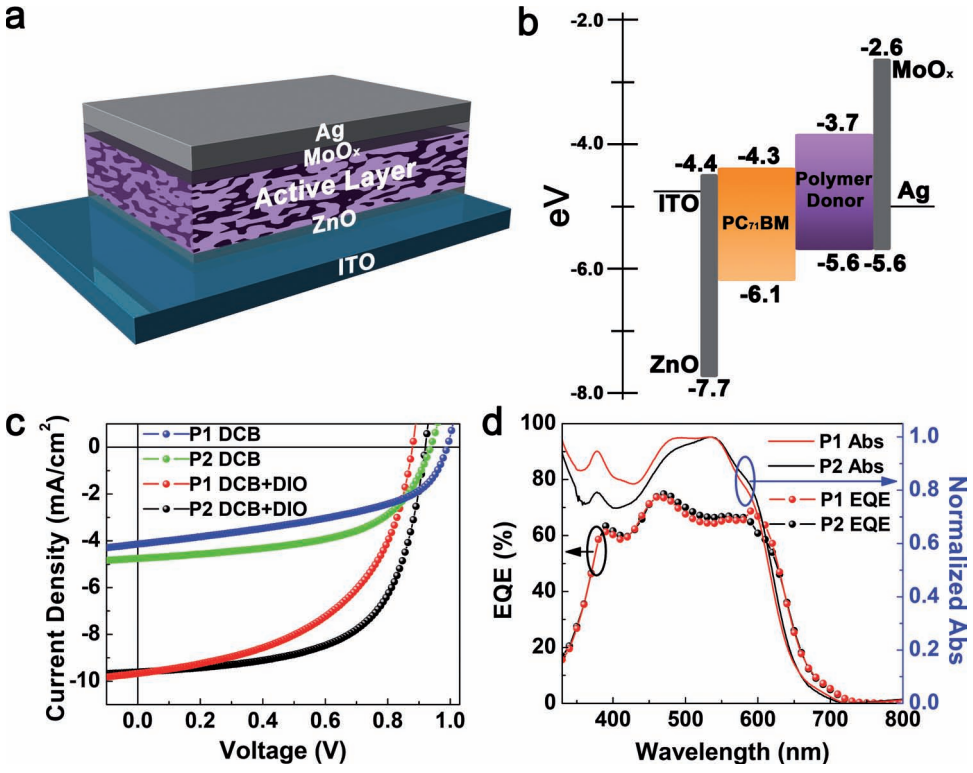

Figure 3. (a) Device structure of an inverted OPV. (b) Energy level diagram in eV of the component materials used in the inverted OPVs. (c) *J*–*V* plots for **P1**:$PC_{71}BM$ (1:1.5) and **P2**:$PC_{71}BM$ (1:1)-based inverted OPVs fabricated with DCB or DCB (97%) + DIO (3%) as processing solvent. (d) EQE plots and absorption spectra for **P1** and **P2**-based inverted solar cells fabricated with DCB (97%) + DIO (3%) as processing solvent.

Table 1. Photovoltaic parameters for **P1** and **P2**-based inverted polymer solar cells in blends with $PC_{71}BM$.

Polymer:$PC_{71}BM$		Solvent	Thickness [nm]	V_{oc} [V]	J_{sc} [mA/cm^2]	*FF* (%)	PCE (%)
P1	1:1.5	DCB	95	0.992	4.16	47.9	1.98
P2	1:1	DCB	100	0.940	4.76	56.3	2.52
P1	1:1.5	DCB+DIO[a)]	95	0.876	9.69	51.8	4.39
P2	1:1	DCB+DIO[a)]	100	0.922	9.62	62.0	5.50

[a)]Device fabricated from DCB:DIO (97%:3%, v/v).

yield lower PCEs (Table S2), which may reflect suboptimal film morphologies and/or decreased optical absorption of the active layer for the cells due to increased $PC_{71}BM$ loading. The variation of the polymer/$PC_{71}BM$ blend ratios leads to substantial variation of the V_{oc}s in the **P1**-based solar cells. Such differences in V_{oc}s have been observed in other polymer solar cells.[13,38] Although OPV V_{oc}s are principally determined by the energy offset between the acceptor LUMO and donor HOMO,[17] other factors greatly affect V_{oc}s such as the active layer morphology,[39] the surface composition between the active layer and the electrode,[38] and interfacial dipole moments.[40] In comparison to the devices fabricated without DIO, the enhanced device performance is mainly due to increases in J_{sc} and a slight increase in *FF*. The addition of DIO also leads to decreased V_{oc}s. Thus, V_{oc} falls by ~0.12 V for the **P1**-based solar cells, while the change of V_{oc} (~0.02 V) in the **P2**-based cells is smaller (Table 1). The fall in V_{oc}s likely reflects the lowering of charge transfer state energies upon additive addition.[41] Furthermore, thermal annealing is found to reduce device performance (Figure S6 and Table S3). For instance, thermal annealing of **P2**-based solar cells at 100 °C for 20 min before deposition of MoO_3/Ag electrode degrades device PCE from 5.50% to 3.97%. The EQEs across the 400 to 600 nm range are generally above 60% in the optimized **P1**- and **P2**-based OPVs, consistent with the optical absorption spectra of blend films prepared under the same conditions as the actual OPVs. Note that the measured J_{sc}s are in a good agreement with external quantum efficiency (EQE) measurements (Figure 3d). Thus, the EQE-derived J_{sc}s of 9.35 and 9.30 mA/cm^2 for the **P1** and **P2**-based solar cells, respectively, are within the stated 4% error of the J_{sc} values obtained from *J*–*V* measurements.

The charge transport properties of **P1** and **P2** films were evaluated in bottom-gate/top-contact organic thin-film transistors (OTFTs).[30] Films were deposited by spin-coating 10 mg/mL polymer solutions onto the hexamethyldisilazane (HMDS)-modified Si (001) wafers having 300 nm thermally grown SiO_2 dielectric layers (see the Supporting Information for details). Based on the transfer curves, the derived hole mobilities are 1.2×10^{-4} cm^{2}V^{-1}s^{-1} and 2.8×10^{-4} cm^{2}V^{-1}s^{-1} for **P1** and **P2**-based OTFTs, respectively. The mobilities measured by the space charge limited current (SCLC) technique are 5.5×10^{-5} and 1.9×10^{-4} cm^{2}V^{-1}s^{-1} for **P1** and **P2**, respectively (Figure S7). Thus, the linear alkyl substituent on the imide group in **P2** results in a higher mobility versus **P1**. The relatively low mobilities in both polymers are in accord with the amorphous film microstructures discussed above (Figure S3). To understand the evolution of OPV device performance, the film morphology of the polymer/$PC_{71}BM$ active layers was also investigated by tapping mode AFM and TEM for blend films produced with and without additives. For the films produced without DIO, the AFM topographic images reveal predominantly phase-segregated morphologies for the **P1**/$PC_{71}BM$ and **P2**/$PC_{71}BM$ blends (**Figure 4**a and 4c). The dark regions in the TEM images as shown in inset of Figure 4a and 4c confirm large $PC_{71}BM$ domain sizes–far larger than typical exciton diffusion lengths (~10 nm).[9] Consequently, poor exciton dissociation and low current density are expected. In contrast, significantly more homogeneous morphologies are found for **P1**/$PC_{71}BM$ and **P2**/$PC_{71}BM$ films processed with DIO. Here, nanoscale phase separation and bicontinuous interpenetrating networks as shown in Figures 4b and 4d result in more efficient charge separation and transport, leading to more than doubled J_{sc} (Figure 3c).

In addition to PCE, stability is critical for practical OPV applications. The inverted device structure eliminates the hygroscopic and acidic PEDOT:PSS IFL and reactive low work-function cathodes used in conventional device structures. Thus, metal oxide IFLs on either side of the polymer/$PC_{71}BM$ blend active layer in inverted OPVs can prevent moisture diffusion into the active layer.[10] We monitored the stability of the best-performing cells with PCE = 5.5% in ambient air at 80 °C under constant illumination. The normalized PCEs for the **P2**/$PC_{71}BM$ solar cells as function of the storage time are illustrated in Figure S9. The OPVs evidence significant falls in PCE at early times, assignable to microstructural reorganization[42,43] since optimal cells are achieved without thermal annealing (which maximizes the initial PCE). As a control, degradation of inverted cells fabricated after thermal annealing at 100 °C for 20 min is significantly reduced, which further supports the contention that device performance degradation of cells fabricated without thermal annealing is due to microstructural reorganization of active layer. After 600 hours storage at 80 °C in ambient, the **P2**/$PC_{71}BM$ inverted cell PCEs retain 53% of the initial values. However, for the conventional solar cells, the PCEs degrade 50% after 168 hours storage under the same conditions. Therefore, device stability is greatly improved in the inverted solar cells. Furthermore, the device performance of BTI-based polymers is temporally more stable than P3HT solar cells having a conventional device structure,[44] which can be attributed to the low-lying HOMO levels of BTI-based polymers.

In conclusion, bithiophene imide and benzodithiophene copolymers synthesized via Stille coupling show high molecular weights and good solution processability. The low-lying **P1**

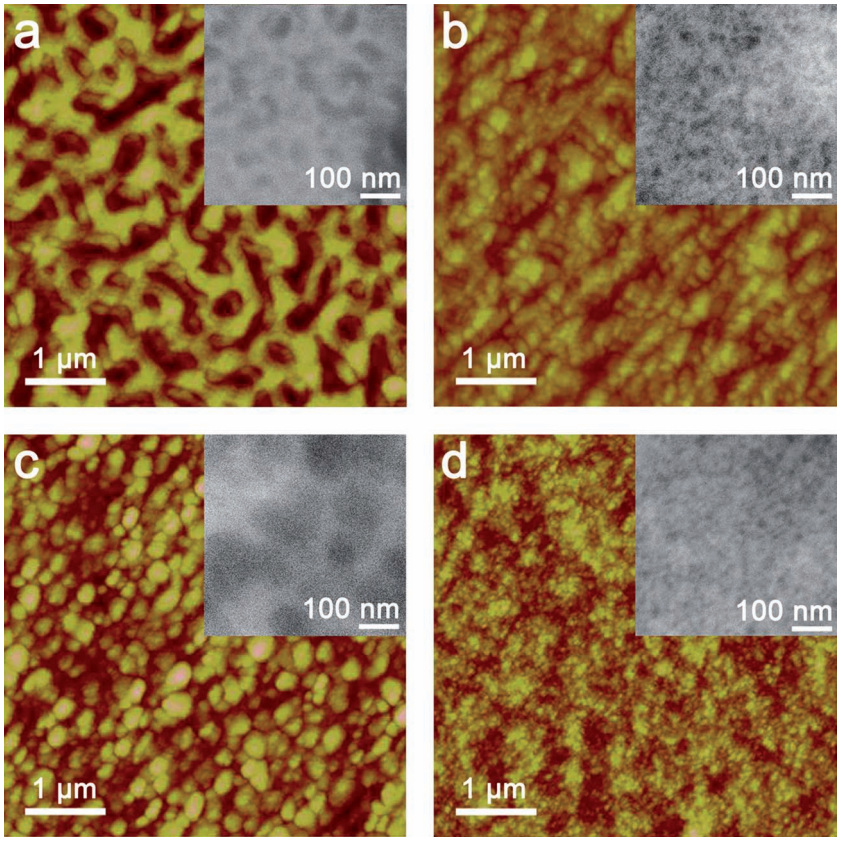

Figure 4. Tapping-mode AFM and TEM images (inset) for (a) **P1**:$PC_{71}BM$ = 1:1.5, DCB as processing solvent. (b) **P1**:$PC_{70}BM$ = 1:1.5, DCB:DIO (97%:3%, v/v) as processing solvent. (c) **P2**:$PC_{71}BM$ = 1:1, DCB as processing solvent. (d) **P2**:$PC_{71}BM$ = 1:1, DCB:DIO (97%:3%, v/v) as processing solvent. (AFM scan area: 5 μm × 5 μm. Note: RMS roughness = 5.82 (a), 5.47 (b) 3.55 (c) and 2.15 nm (d). TEM scan area: 0.5 μm × 0.5 μm)

and **P2** bithiophene imide HOMOs (–5.50 eV – –5.60 eV) lead to high open circuit voltages (>0.9 V) in OPVs. Inverted solar cells having the structure ITO/ZnO/polymer:$PC_{71}BM$/MoO_x/Ag exhibit power conversion efficiencies as high as 5.5%. Due to the low-lying HOMOs and inverted device structures, OPVs fabricated from these bithiophene imide-based polymers exhibit promising device air and thermal stability. As the first bithiophene imide-based polymers for OPV application, these results indicate that bithiophene imide is a very promising building block for polymer OPVs. As a new material in the field, we anticipate further improvements through materials modifications, including side chains, backbones, and molecular weights, as well as device optimization, such as processing additives and interfacial layers, which will be reported in due course.

Experimental Section

Materials and Methods: All chemicals and reagents were purchased from commercial sources and used without further purification. Anhydrous dichloromethane was distilled from calcium hydride, whereas THF, diethyl ether, and toluene were distilled from Na/benzophenone. Unless otherwise stated, all reactions were carried out under inert atmosphere using standard Schlenk techniques. NMR spectra were recorded on Varian Unity Plus 500 (500 MHz, room temperature) or Mercury 400 (400 MHz, high temperature) spectrometers, and chemical shifts are referenced to residual protio-solvent signals. Elemental analyses (EA) were performed by Midwest Microlab (Indianapolis, IN). Polymer molecular weights were determined on a Polymer Laboratories PL-GPC 220 using trichlorobenzene as eluent at 170 °C with polystyrene as a standard. Optical spectra were recorded on a Varian Cary 50 Scan spectrophotometer. The polymer solution absorption spectra were recorded on 10^{-5} M chlorobenzene solutions at room temperature, and polymer film spectra were recorded on films drop-cast from 1 mg/mL chlorobenzene solutions. Thermogravimetric analysis (TGA) was performed on a TA Q50 instrument at a ramp rate of 10 °C/min under N_2 at atmospheric pressure in a Pt crucible. Differential scanning calorimetry (DSC) was performed on TA model DSC 2920 with a heating ramp of 10 °C/min and data are reported from the second heating-cooling cycle. Electrochemistry was measured on a C3 cell stand electrochemical station with BAS Epsilon software (Bioanalytical Systems, Inc., Lafayette, IN). The electrochemical properties of the polymers were investigated as thin films in anhydrous acetonitrile under N_2 at a scan rate of 50 mV/s using 0.1 M tetrakis(*n*-butyl) ammonium hexafluorophosphate ($(n\text{-Bu})_4N{\cdot}PF_6$) as the supporting electrolyte. Pt electrodes were used as both the working and counter electrodes, and an Ag wire was used as the pseudoreference electrode. Polymer films were drop-cast onto the Pt working electrode from a 0.2% (w/w) chlorobenzene solution.

General Procedure for polymer synthesis: An air-free flask was charged with the two monomers (0.2 mmol each), $Pd_2(dba)_3$, and P(*o*-tolyl)$_3$ (1:8, $Pd_2(dba)_3$:P(*o*-tolyl)$_3$ molar ratio; Pd loading = 0.03 equiv.). The flask and its contents were subjected to 3 pump/purge cycles with argon, followed by addition of 8 mL anhydrous toluene. The sealed reaction flask was then stirred at 110 °C for 72 h. Then, 0.1 mL 2-(tributylstanny) thiophene was added and the reaction mixture was stirred at 110 °C for another 12 h. Finally, 0.2 mL 2-bromothiophene was added and the reaction mixture was stirred for another 12 h. After cooling to room temperature, the reaction mixture was dripped into 100 mL of methanol (containing 5 mL 12 N HCl) with vigorous stirring. After 4 h stirring, the polymer was transferred to a thimble. After drying, the crude product was subjected to sequential Soxhlet extraction. After final extraction with chloroform, the polymer solution was precipitated then in 100 mL of methanol with vigorous stirring. The polymer was collected by filtration and dried to afford purple solid as the product.

P1. This product was obtained as purple solid after Soxhlet extraction with methanol, acetone, hexane, dichloromethane, and chloroform (117 mg, 69% yield). M_n = 21.8 kDa, PDI = 3.28. ^{1}H NMR (400 MHz, $C_2D_2Cl_4$, 130 °C, ppm): δ 7.70 (br, 2H), 7.39 (br, 2H), 4.30 (br, 6H), 2.01 (br, 3H), 1.63-0.97 (m, 32H), 1.20 (b, 12H), 0.96 (b, 6H). Anal. Calcd for $C_{48}H_{63}NO_4S_4$ (%): C, 68.12; H, 7.50; N, 1.66. Found (%): C, 68.34; H, 7.39; N, 1.71.

P2. This product was obtained as purple solid after Soxhlet extraction with methanol, acetone, hexane, and chloroform (191 mg, 94% yield). M_n = 34.0 kDa, PDI = 2.95. ^{1}H NMR (400 MHz, $C_2D_2Cl_4$, 130 °C, ppm): δ 7.77 (br, 2H), 7.41 (br, 2H), 4.33 (br, 6H), 2.07 (br, 5H), 1.63-0.97 (m, 60H), 0.97 (b, 12H). Anal. Calcd for $C_{60}H_{87}NO_4S_4$ (%): C, 71.03; H, 8.64; N, 1.38. Found (%): C, 71.43; H, 8.39; N, 1.52.

Solar Cell Fabrication and Characterization: Pre-patterned ITO-coated glass (Thin Film Devices, Inc.) with a series resistance of ~8Ω/□ was

used as the substrate. It was cleaned by sequential sonication in hexane, DI water, methanol, isopropanol, and acetone, and finally UV/ozone treated (Jelight Co.) for 30 min. For the fabrication of inverted solar cells, ZnO electron transport/hole blocking layer was prepared by spin-coating at 5000 rpm from a ZnO precursor solution prepared from 0.5 M zinc acetate dehydrate in 0.5 M monoethanolamine and 2-methoxyethanol under N_2. After cleaning the electrical contacts, substrates were immediately baked in air 150 °C for 5 min. The films were then rinsed with DI water, isopropanol, and acetone, and then dried in a glovebox. Active layer solutions were prepared in DCB or DCB/DIO (97%/3%, v/v) (polymer concentration: 10 mg/mL). For optimum performance **P1** and **P2** devices, active layers were spin-coated at 1250 rpm and 1000 rpm to obtain thicknesses of 95 nm and 100 nm, respectively. Thin layers of 5 nm MoO_x and 100 nm of Ag were then thermally evaporated through a shadow mask at ~10^{-6} Torr. For the fabrication of conventional solar cells, PEDOT:PSS (Clevios P VP Al 4083) was spun-cast at 5000 rpm for 30 sec and annealed at 150 °C. Active layers are prepared under the same conditions as the inverted solar cells. LiF(1.0 nm)/Al(100 nm) were then thermally evaporated through a shadow mask at ~10^{-6} Torr. Device *I–V* characteristics measured under AM1.5G light (100 mW/cm^2) using the Xe arc lamp of a Spectra-Nova Class A solar simulator. The light intensity was calibrated using an NREL-certified monocrystalline Si diode coupled to a KG3 filter to bring spectral mismatch to unity. Four-point contact measurements were performed and electrical characterizations were measured with a Keithley 2400 unit. The area of all devices was 6 mm^2, and an aperture with size of 6 mm^2 was used on top of cells during measurements. EQEs were characterized using an Oriel model QE-PV-SI instrument equipped with an NIST-certified Si diode. Monochromatic light was generated from an Oriel 300W lamp source.

AFM, XRD, and TEM: AFM measurements were performed by using a Dimension Icon Scanning Probe Microscope (Veeco) in tapping mode. XRD measurements were performed on an 18 kW Rigaku ATXG diffractometer using a multilayer parabolic mirror, a NaI scintillation detector, and X-rays of wavelength λ = 1.541 Å. TEM specimens were prepared following identical conditions as the actual devices, but were drop cast onto 2 mm × 2 mm NaCl (100) polished substrates (MTI Corp.). After drying, substrates were transferred to DI water and the floated films were transferred to TEM grids (Ted Pella, Inc.). TEM images were obtained on Hitachi HD-2300A STEM.

Supporting Information

Supporting Information is available from the Wiley Online Library or from the author.

Acknowledgements

N. Z and X. G. contributed equally to this work. This material is based upon work supported as part of the ANSER Center, an Energy Frontier Research Center funded by the U.S. Department of Energy, Office of Science, and Office of Basic Energy Sciences under Award Number DE-SC0001059. We thank AFOSR (FA9550-08-1-0331) and the NSF-MRSEC program through the Northwestern University Materials Research Science and Engineering Center for characterization facilities (DMR-0520513). XRD measurements are performed at J. B. Cohen X-Ray Diffraction Facility supported by the MRSEC program of the National Science Foundation (DMR-1121262) at the Materials Research Center of Northwestern University. TEM measurements were performed at the EPIC facility, located in NUANCE Center at Northwestern University. NUANCE Center is supported by NSF-NSEC, NSF-MRSEC, Keck Foundation, the State of Illinois, and Northwestern University. R. P. O. acknowledges funding from the European Community's Seventh Framework Programme through a Marie Curie International Fellowship (Grant Agreement 234808).

Received: October 13, 2011
Revised: January 30, 2012
Published online: March 26, 2012

[1] S. Günes, H. Neugebauer, N. S. Sariciftci, *Chem. Rev.* **2007**, *107*, 1324.
[2] B. C. Thompson, J. M. J. Fréchet, *Angew. Chem., Int. Ed.* **2008**, *47*, 58.
[3] Y.-J. Cheng, S.-H. Yang, C.-S. Hsu, *Chem. Rev.* **2009**, *109*, 5868.
[4] A. Facchetti, *Chem. Mater.* **2011**, *23*, 733.
[5] P. L. T. Boudreault, A. Najari, M. Leclerc, *Chem. Mater.* **2011**, *23*, 456.
[6] a) M. D. Irwin, D. B. Buchholz, A. W. Hains, R. P. H. Chang, T. J. Marks, *Proc. Natl. Acad. Sci. U.S.A.* **2008**, *105*, 2783; b) M. D. Irwin, J. D. Servaites, D. B. Buchholz, B. J. Leever, J. Liu, J. D. Emery, M. Zhang, J.-H. Song, M. F. Durstock, A. J. Freeman, M. J. Bedzyk, M. C. Hersam, R. P. H. Chang, M. A. Ratner, T. J. Marks, *Chem. Mater.* **2011**, *23*, 2218.
[7] L. Motiei, Y. Yao, J. Choudhury, H. Yan, T. J. Marks, M. E. van der Boom, A. Facchetti, *J. Am. Chem. Soc.* **2010**, *132*, 12528.
[8] W. Ma, C. Yang, X. Gong, K. Lee, A. J. Heeger, *Adv. Funct. Mater.* **2005**, *15*, 1617.
[9] J. Peet, A. J. Heeger, G. C. Bazan, *Acc. Chem. Res.* **2009**, *42*, 1700.
[10] Y. Sun, J. H. Seo, C. J. Takacs, J. Seifter, A. J. Heeger, *Adv. Mater.* **2011**, *23*, 1679.
[11] C. M. Amb, S. Chen, K. R. Graham, J. Subbiah, C. E. Small, F. So, J. R. Reynolds, *J. Am. Chem. Soc.* **2011**, *133*, 10062.
[12] Y. Liang, Z. Xu, J. Xia, S.-T. Tsai, Y. Wu, G. Li, C. Ray, L. Yu, *Adv. Mater.* **2010**, *22*, E135.
[13] T.-Y. Chu, J. Lu, S. Beaupré, Y. Zhang, J.-R. Pouliot, S. Wakim, J. Zhou, M. Leclerc, Z. Li, J. Ding, Y. Tao, *J. Am. Chem. Soc.* **2011**, *133*, 4250.
[14] Z. He, C. Zhong, X. Huang, W.-Y. Wong, H. Wu, L. Chen, S. Su, Y. Cao, *Adv. Mater.* **2011**, *23*, 4636.
[15] M. A. Green, K. Emery, Y. Hishikawa, W. Warta, *Prog. Photovoltaics* **2011**, *18*, 144.
[16] J. Roncali, *Chem. Rev.* **1997**, *97*, 173.
[17] M. C. Scharber, D. Wuhlbacher, M. Koppe, P. Denk, C. Waldauf, A. J. Heeger, C. L. Brabec, *Adv. Mater.* **2006**, *18*, 789.
[18] Y. Liang, Y. Wu, D. Feng, S.-T. Tsai, H.-J. Son, G. Li, L. Yu, *J. Am. Chem. Soc.* **2009**, *131*, 56.
[19] Y. Liang, D. Feng, Y. Wu, S.-T. Tsai, G. Li, C. Ray, L. Yu, *J. Am. Chem. Soc.* **2009**, *131*, 7792.
[20] Y. Zou, A. Najari, P. Berrouard, S. Beaupré, B. R. Aïch, Y. Tao, M. Leclerc, *J. Am. Chem. Soc.* **2010**, *132*, 5330.
[21] D. Gendron, M. Leclerc, *Energy Environ. Sci.* **2011**, *4*, 1225.
[22] C. Piliego, T. W. Holcombe, J. D. Douglas, C. H. Woo, P. M. Beaujuge, J. M. J. Fréchet, *J. Am. Chem. Soc.* **2010**, *132*, 7595.
[23] X. Guo, H. Xin, F. S. Kim, A. D. T. Liyanage, S. A. Jenekhe, M. D. Watson, *Macromolecules* **2011**, *44*, 269.
[24] T.-Y. Chu, J. Lu, S. Beaupré, Y. Zhang, J.-R. Pouliot, S. Wakim, J. Zhou, M. Leclerc, Z. Li, J. Ding, Y. Tao, *J. Am. Chem. Soc.* **2011**, *133*, 4250.
[25] J. A. Letizia, M. R. Salata, C. M. Tribout, A. Facchetti, M. A. Ratner, T. J. Marks, *J. Am. Chem. Soc.* **2008**, *130*, 9679.
[26] X. Guo, R. P. Ortiz, Y. Zheng, Y. Hu, Y. Y. Noh, K. J. Baeg, A. Facchetti, T. J. Marks, *J. Am. Chem. Soc.* **2011**, *133*, 1405.
[27] L. Huo, J. Hou, *Polym. Chemistry.* **2011**, *2*, 2453.

[28] G. Zhang, Y. Fu, Q. Zhang, Z. Xie, *Chem. Commun.* **2010**, *46*, 4997.
[29] J. K. Park, J. Jo, J. H. Seo, J. S. Moon, Y. D. Park, K. Lee, A. J. Heeger, G. C. Bazan, *Adv. Mater.* **2011**, *23*, 2430.
[30] X. Guo, R. P. Ortiz, Y. Zheng, M.-G. Kim, S. Zhang, Y. Hu, G. Lu, A. Facchetti, T. J. Marks, *J. Am. Chem. Soc.* **2011**, *133*, 13685.
[31] A. R. Murphy, J. Liu, C. Luscombe, D. Kavulak, J. M. J. Fréchet, R. J. Kline, M. D. McGehee, *Chem. Mater.* **2005**, *17*, 4892.
[32] J. Kim, T. M. Swager, *Nature* **2001**, *411*, 1030
[33] E. Ahmed, S. Subramaniyan, F. S. Kim, H. Xin, S. A. Jenekhe, *Macromolecules* **2011**, *44*, 7207.
[34] A. L. Roest, J. J. Kelly, D. Vanmaekelbergh, E. A. Meulenkamp, *Phys. Rev. Lett.* **2002**, *89*, 036801.
[35] S. K. Hau, H. L. Yip, H. Ma, A. K. Y. Jen, *Appl. Phys. Lett.* **2008**, *93*, 233304.
[36] C.-H. Chou, W. L. Kwan, Z. Hong, L.-M. Chen, Y. Yang, *Adv. Mater.* **2011**, *23*, 1282.
[37] The exact role of MoO_3 as anode interfacial layer is not yet fully understood; further in-depth investigation is required to elucidate its electronic nature. Besides the explanation of role of MoO_3 in [36], altanative one is recently proposed by K. Kröger, S. Hamwi, J. Meyer, T. Riedl, W. Kowalsky, A. Kahn, *Appl. Phys. Lett.* **2009**, *95*, 123301.
[38] C. R. McNeill, J. J. M. Halls, R. Wilson, G. L. Whiting, S. Berkebile, M. G. Ramsey, R. H. Friend, N. C. Greenham, *Adv. Funct. Mater.* **2008**, *18*, 2309.
[39] J. Liu, Y. J. Shi, Y. Yang, *Adv. Funct. Mater.* **2001**, *11*, 420.
[40] A. Tada, Y. Geng, Q. Wei, K. Hashimoto, K. Tajima, *Nat. Mater.* **2011**, *10*, 450.
[41] D. Di Nuzzo, A. Aguirre, M. Shahid, V. S. Gevaerts, S. C. J. Meskers, R. A. J. Janssen, *Adv. Mater.* **2010**, *22*, 4321.
[42] K. Sivula, C. K. Luscombe, B. C. Thompson, J. M. J. Fréchet, *J. Am. Chem. Soc.* **2006**, *128*, 13988.
[43] G. Griffini, J. D. Douglas, C. Piliego, T. W. Holcombe, S. Turri, J. M. J. Fréchet, J. L. Mynar, *Adv. Mater.* **2011**, *23*, 1660.
[44] M. Wang, Q. Tang, J. An, F. Xie, J. Chen, S. Zheng, K. Y. Wong, Q. Miao, J. Xu, *ACS Appl. Mater. Interfaces* **2010**, *2*, 2699